Modeling of SiO_2 Deposition in Porous Vycor: Effects of Pore Network Connectivity

Michael Tsapatsis
Dept. of Chemical Engineering, California Institute of Technology, Pasadena, CA 91125

George Gavalas
Dept. of Chemical Engineering, California Institute of Technology, Pasadena, CA 91125

A mathematical model developed for SiO_2 deposition in porous Vycor glass using $SiCl_4$ hydrolysis describes reaction, diffusion and evolution of the pore structure due to accumulation of the solid product. The deposition reaction is described by transient heterogeneous kinetics in terms of the concentrations of silanol and chloride groups in the product layer as well as those of the gaseous reactants. For typical deposition conditions the pseudo steady-state approximation for surface species could lead to erroneous predictions. Pore structure evolution is modeled by incorporating results of percolation theory. For this purpose the porous glass is represented by a Bethe lattice with coordination number 3 and alternatively by a decorated Bethe lattice in which each bond is replaced by a composite bond consisting of two bonds in series. The second network can capture the effect of pore radius variation along a single pore. For the decorated lattice, pore connectivity interruption at a higher void fraction leads to thinner deposits and shorter deposition times for pore plugging compared to the corresponding ones for the simple lattice.

Introduction

Chemical vapor deposition (CVD) has been used by several research groups to prepare oxide membranes supported on porous tubes. The modeling of the deposition process has also received considerable attention. Generally speaking there are two major aspects that must be addressed in this modeling, namely, the kinetics of the CVD reactions and the evolution of the porous structure. Previous work (Yortsos and Sharma, 1986; Reyes and Jensen, 1987; Zarkantis et al., 1990; Efthimiadis and Sotirchos, 1993) has demonstrated the importance of network connectivity effects on gas–solids reactions, such as lime sulfation involving expansion of the solid volume with a corresponding constriction of the pore space. The same phenomenon is relevant in the CVD of SiO_2, ZrO_2, and so forth, on porous supports and, in fact, it plays a key role on the structure of the resulting membrane layer. It is therefore the main purpose of this article to include pore network effects in the modeling of SiO_2 membrane CVD, extending our previous work on this subject. In addition, we introduce some improvements in the kinetic model used previously (Tsapatsis and Gavalas, 1992).

Previous modeling studies of membrane CVD (Carolan and Michaels, 1987; Tsapatsis and Gavalas, 1992; Lin and Burggraaf, 1992) have not considered pore connectivity effects. The issue of concern here is that during deposition segments of the pore space become isolated and inaccessible to the reactants. When this process has progressed far enough, a transition point is reached, called the percolation threshold, at which the properties of the porous medium suddenly change because the previously connected sample-spanning network of open pores suddenly becomes disconnected. The experimental implications of these phenomena are manifested in recent results from transmission electron microscopy (Tsapatsis and Gavalas, 1994) and thermogravimetric experiments (Kim and Gavalas, 1994), revealing that at the end of deposition a substantial amount of porosity (up to 1/3 of the initial) remains that is open but inaccessible to reac-

Current address of M. Tsapatsis: Dept. of Chemical Engineering, Univ. of Massachusetts, Amherst, MA 01003.

tants. Although trapped, this residual porosity can modify significantly the permeabilities of hydrogen and other gases (Tsapatsis and Gavalas, 1994).

Mohanty et al. (1982) were the first to describe reaction and transport in a porous medium using percolation concepts by representing the porous medium as a network of interconnected pores that can be blocked at random. More detailed treatments that follow more consistently the evolution of connectivity have also been developed (Mace and Wei, 1991).

Sahimi (1985) and Sahimi and Tsotsis (1985) were the first to point out an important difference between random percolation and deposition processes in their treatment of catalyst deactivation. In random percolation a pore is picked at random and is blocked regardless of whether or not it can be reached by reactants. In reality isolated pores cannot be reached by reactants and therefore they cannot become blocked. This trapping effect [the term is after Sahimi (1985)] was treated elegantly by Yu and Sotirchos (1987) in their analysis of gas–solid reactions and is also discussed here in the following section. Yu and Sotirchos (1987) and Yortsos and Sharma (1986) have studied gas–solid reactions with pore closure by solving the continuum equations of diffusion and reaction using random percolation to estimate the effective diffusivity. Arbabi and Sahimi (1991) developed lattice models that do not rely on continuum equations. Matters regarding continuum vs. network description of pore structures are fully discussed by Sahimi et al. (1990). Here we only note that the development of the deposit profile in membrane deposition takes place mainly where the pore structure is far from its percolation threshold, hence a continuum description should give a reasonable description of structure evolution.

Therefore, we implement the model developed by Yu and Sotirchos (1987) to study the effect of connectivity evolution on the deposit profile and on the extent of deposition required to block the pores of the Vycor substrate. A new element introduced here is the use of a decorated lattice to take into account the pronounced effect of cross-sectional variation along the axis of a single pore segment. The final permeation properties of the membrane depend on the microstructure of the composite material very close to the percolation threshold where long correlation lengths undermine the continuum description. Therefore, this second and more demanding problem is not examined here.

Reviewing now previous kinetic modeling of SiO_2 and other oxides in porous substrates we note first an early study of Carolan and Michaels (1987). These authors have modeled the deposition of yttria-stabilized-zirconia by chloride hydrolysis by a phenomenological reaction rate of the form:

$$r = k\,(C_{\text{chloride}})^a\,(C_{\text{water}})^b. \tag{1}$$

In their model the variation of pore size and diffusivity was not taken into account in formulating the transport equations. Lin and Burggraaf (1992) developed a more realistic description of the deposition process using a similar rate expression but taking into account the effect of pore constriction on diffusion coefficients. A pseudohomogeneous description in terms of macroscopic diffusivities and tortuosity factors was used to relate the diffusivity with the average pore radius. Xomeritakis and Lin (1994a,b) developed semianalytical solutions to describe the evolution of the deposit profiles. For this purpose they used a phenomenological model to account for diffusion, reaction, and pore geometry changes, but did not consider the evolution of connectivity of the porous structure engendered by the deposition.

We have prepared hydrogen permselective membranes by CVD of SiO_2, TiO_2, and other films on porous Vycor tubes. Characterization of these oxide layers has been presented elsewhere (Tsapatsis and Gavalas, 1992, 1994). The former article presented a model describing the deposition of SiO_2 in porous Vycor in an opposing reactants geometry (ORG) where the chloride and water reactants are introduced from opposing sides of the Vycor substrate. The kinetics were described by the following simplified heterogeneous mechanism:

$$\text{Si–OH}(s) + \text{SiCl}_4(g) = 3\,\text{Si–Cl}(s) + \text{HCl}(g) \tag{2}$$

$$\text{Si–Cl}(s) + \text{H}_2\text{O}(g) = \text{Si–OH}(s) + \text{HCl}(g) \tag{3}$$

$$\text{Si–OH}(s) + \text{Si–OH}(s) = \text{Si–O–Si}(s) + \text{H}_2\text{O}(g) \tag{4}$$

$$\text{Si–OH}(s) + \text{Si–Cl}(s) = \text{Si–O–Si}(s) + \text{HCl}(g), \tag{5}$$

where Si–OH(s) represents a surface hydroxyl (silanol), Si–Cl(s) a surface chloride, and Si–O–Si(s) a siloxane bridge on the solid. This notation counts surface –OH and –Cl sites and not silicon atoms. The model gave predictions of deposit profiles in qualitative agreement with experimental results. It was noted that transient kinetics like those represented by Eqs. 2–5 are essential for porous substrates like Vycor having a pore diameter of about 4 nm. Steady-state kinetics, however, like those of Eq. 1 are probably adequate for describing deposition in larger pores, for example, pore diameter larger than 20 nm. Here we use some recent kinetic results (Kim and Gavalas, 1994) to simplify the reaction scheme and eliminate the uncertainty involved in several kinetic parameters used in the previous model.

Model Formulation

Kinetics

The deposition of silica on Vycor glass will be described by Eqs. 2 to 5. In our previous treatment (Tsapatsis and Gavalas, 1992) we assumed that all hydroxyl (silanols) and chloride sites in the deposit layer are equally reactive in silylation, reaction 2, and hydrolysis, reaction 3, respectively. Here we wish to recognize that reactions 2 and 3 with hydroxyl or chloride sites located below the surface layer of the deposit are strongly hindered. Differences in reactivity due to steric effects have also been observed among hydroxyl sites on the original surface of Vycor (Kim and Gavalas, 1994), but these will not be considered here. To provide a rigorous description of reactivity differences due to steric hindrance is impractical, therefore here we shall adopt an empirical approach dividing the hydroxyl and chloride sites into a superficial group of uniform reactivity and a subsurface group of zero reactivity. Denoting by A the variable pore surface (cm^2) and by S_{OH}, S_{Cl}, the surface concentrations of –OH and –Cl sites (mol/cm^2) we shall assume that because of steric effects $S_{OH} + S_{Cl}$ cannot exceed some maximum value S^* (mol/cm^2). Consider now the pore surface area A (cm^2) and the surface concentrations

of OH and Cl sites denoted by S_{OH}, S_{Cl} (mol/cm^2). All three quantities vary with time.

The balance equations for the surface –OH and –Cl groups can then be written as follows:

$$\frac{\partial(AS_{OH})}{\partial t} = -Ak_1C_1S_{OH} + Ak_2C_2S_{Cl} - FS_{OH} \quad (6)$$

$$\frac{\partial(AS_{Cl})}{\partial t} = 3Ak_1C_1S_{OH} - Ak_2C_2S_{Cl} - FS_{Cl} \quad (7)$$

where C_1, C_2 are the gas phase concentrations of $SiCl_4$ and H_2O.

The last term in Eqs. 6 and 7 require some explanation. Initially, the total concentration of surface sites will usually be below the maximum value S^*. Under these circumstances the last terms FS_{OH}, FS_{Cl} should be zero, that is,

$$F = 0 \quad \text{for} \quad S_{OH} + S_{Cl} < S^*. \quad (8)$$

At some point after the beginning of the reaction the total surface sites reach the maximum value S^*. After that any generation of –OH or –Cl groups must be accompanied by loss of existing surface groups to the interior in order to maintain the total number at the value S^*. Adding Eqs. 6 and 7 and setting $\partial(S_{OH} + S_{Cl})/\partial t = 0$, we obtain

$$F = \frac{2k_1C_1AS_{OH}}{S^*} - \frac{\partial A}{\partial t} \quad \text{for} \quad S_{OH} + S_{Cl} = S^*. \quad (9)$$

The maximum surface concentration S^* is an empirical parameter in the model, but should be on the order of the number of sites in a monolayer.

Equations 6 and 7 can now be rewritten using Eqs. 8 and 9 (after the value S^* has been reached by $S_{OH} + S_{Cl}$):

$$\frac{\partial S_{OH}}{\partial t} = -k_1C_1S_{OH} + k_2C_2S_{Cl} - \frac{2k_1}{S^*}C_1S_{OH}^2 \quad (10)$$

$$\frac{\partial S_{Cl}}{\partial t} = 3k_1C_1S_{OH} - k_2C_2S_{Cl} - \frac{2k_1}{S^*}C_1S_{Cl}S_{OH}. \quad (11)$$

These equations describe the evolution of the surface concentrations of reactive sites at each location. The concentrations of the gaseous reactants satisfy the familiar reaction–diffusion equations:

$$\frac{\partial}{\partial x}\left(D_1\frac{\partial C_1}{\partial x}\right) = k_1C_1AS_{OH} \quad (12)$$

$$\frac{\partial}{\partial x}\left(D_2\frac{\partial C_2}{\partial x}\right) = k_2C_2AS_{Cl}. \quad (13)$$

The accumulation terms $\partial C_1/\partial t$, $\partial C_2/\partial t$ have been omitted from Eqs. 12 and 13 as being much smaller than the other terms backed by a simple scaling analysis given in the Appendix.

In Eqs. 12 and 13 the diffusion coefficients D_1, D_2 and the surface area vary with time and position. We shall be able to express these three quantities as functions of the local thickness of the deposit layer q (cm). This thickness grows with time according to

$$\frac{\partial q}{\partial t} = vk_1C_1S_{OH}, \quad (14)$$

where v is the molar volume in the deposit (cm^3/mol).

Equations 10–14 are associated with the initial and boundary conditions

$$t = 0: \quad S_{OH} = S_{OH}^0, \quad S_{Cl} = S_{Cl}^0, \quad q = q^0 \quad (15)$$

$$x = 0: \quad l_1(C_{10} - C_1) = -D_1\frac{\partial C_1}{\partial x} \quad (16)$$

$$l_2(C_{20} - C_2) = -D_2\frac{\partial C_2}{\partial x} \quad (17)$$

$$x = L: \quad l_1'(C_{10}' - C_1) = D_1\frac{\partial C_1}{\partial x} \quad (18)$$

$$l_2'(C_{20}' - C_2) = D_2\frac{\partial C_2}{\partial x}. \quad (19)$$

Here the unprimed quantities refer to the chloride side (tube interior) and the primed quantities to the water side (annulus). Since very little water survives the reaction zone to enter the tube interior and very little chloride enters the annulus, we can set to an approximation $C_{10}' = 0$, $C_{20} = 0$. Finally $C_{10} = C_1^0$ and $C_{20}' = C_2^0$ where, C_1^0, C_2^0 the concentrations of chloride and water at the bubblers.

Connectivity considerations

As mentioned in the introduction, during deposition, the pore space progressively disintegrates into isolated pore clusters. Each of these clusters contains pores that are closed and pores that are still open but cannot react anymore because of their inaccessibility to the reactant gases. Along with this real process of connectivity evolution it is convenient to consider the hypothetical process wherein all open pores continue to react whether or not they are accessible to the reactant gases. For brevity the real process will be called *process with trapping*, and the hypothetical process will be called *process without trapping*.

As will be seen below, the surface area accessible to reaction and the effective diffusion coefficients of the reactant gases can be calculated in a simple fashion by following the process without trapping. Calculation of the deposit volume fraction and distribution, however, requires careful consideration of the process with trapping that involves a subtle accounting of the number of radius of pores that are closed, open and accessible, and open and inaccessible.

Connectivity effects on diffusion coefficients are most conveniently described by lattice models. Standard lattice models are unable to take into account variation of the pore (bond) cross-section between points of confluence (sites). This limitation can be removed by the use of "decorated" lattices, where a compound bond [a "bond graph"(Fisher and Essam, 1961)] can be assigned between each adjacent pair of sites. We have found that a decorated lattice can have quite different connectivity evolution than a simple lattice of the same

bond conductance distribution. On the other hand, the complexity of the equations describing the evolution of a decorated lattice increases rapidly with the size of the compound bond. In the following simulations we therefore use the simplest possible decorated lattice wherein each compound bond consists of two simple bonds in series. First, the equations are presented for a "nondecorated" (simple) lattice and then the changes needed for a decorated lattice are provided.

Simple lattices

The porous medium is represented by a network of bonds and sites with coordination number z. We assign negligible volume to the sites and a cylindrical capillary of constant length, l, and radius to each bond. Capillary radius and capillary length are distributed randomly and independently of each other. Thus the number fraction of pores of a certain radius is equal to their length fraction. As pointed out by Sotirchos and Zarkanitis (1993) in their development of models with distributed pore radius and length, the assumption of uniform pore length is a good approximation for solids with a narrow pore-size distribution. Yu and Sotirchos (1987) developed models for both discrete and continuous pore-size distribution. Here a discrete pore-size distribution is used consisting of the radii:

$$R_{0\min} = R_{01} < R_{02} < \cdots R_{0N} = R_{0\max}$$

with lengths $l_{01}, l_{02}, \ldots, l_{0N}$ and total length

$$L_0 = \sum_{i=1}^{N} l_{0i}.$$

A pore will be regarded as closed when its radius declines to a specific value r^*. This value is somewhat arbitrary but can be chosen, for example, as the kinetic radius of the larger of the reactant molecules, in the present problem $SiCl_4$. For simplicity it is assumed that the diffusion of $SiCl_4$ is negligible in pores of radius r^*. At any given location in the porous material, let t_j be the time at which the open accessible pores with initial radius R_{0j} become closed due to the chemical reaction, and let $l^a_{(i,j)}$ be the length of open and accessible pores of initial radius R_{0i} immediately after the pores with initial radius R_{0j} close (at time t_j). Similarly, $l^n_{(i,j)}$ is defined as the corresponding length of open inaccessible pores. At time t with $t_j < t < t_{j+1}$ $(R_{0j} < q < R_{0j+1})$ one has open and accessible pores of radii

$$R_{0j+1} - q, \quad R_{0j+2} - q, \quad \ldots, \quad R_{0N} - q$$

and lengths

$$l^a_{(j+1,j)}, \quad l^a_{(j+2,j)}, \quad \ldots, \quad l^a_{(N,j)}$$

and j groups of inaccessible pores with radii

$$\{R_{02} - (R_{01} - r^*), \ldots, R_{0N} - (R_{01} - r^*)\},$$
$$\{R_{03} - (R_{02} - r^*), \ldots, R_{0N} - (R_{02} - r^*)\}, \ldots,$$
$$\{R_{0j+1} - (R_{0j} - r^*), \ldots, R_{0N} - (R_{0j} - r^*)\}$$

and lengths

$$\{l^n_{(2,1)}, \ldots, l^n_{(N,1)}\}, \{l^n_{(3,2)}, \ldots, l^n_{(N,2)}\}, \ldots,$$
$$\{l^n_{(j+1,j)}, \ldots, l^n_{(N,j)}\}.$$

At t_j all open accessible pores with initial radius R_{0j} become closed having acquired radius r^* and lengths $l^a_{(j,j-1)}$. The fraction of open pores (accessible and inaccessible) $X(t_j)$ is then given by

$$X(t_j) = 1 - \frac{\sum_{i=1}^{j} l^a_{(i,i-1)}}{L_0}, \tag{20}$$

where the sum represents all the pores that became closed at $t_1, \ldots, t_j$. Percolation theory can be used to determine the fraction of pores that are open and accessible (accessibility function) as a function of the fraction of all open pores assuming a spatially random distribution of pores. The accessibility function has been computed for several common lattices. These results can be used to calculate the open-accessible pores for the hypothetical process without trapping, for this process involves a spatially random distribution. For this purpose let X, X^* be the fraction of open pores in the process with and without trapping, respectively. Clearly $X > X^*$, because an open inaccessible pore cannot become closed due to the trapping effect, while it can be closed in the process without trapping used to define X^*. The important point to be noted (Yu and Sotirchos, 1987) is that open and accessible pores in the process with trapping are also open and accessible in the process without trapping and vice versa. Therefore, the open and accessible pores at t_j will have lengths:

$$l^a_{(j+n,j)} = l^a_{(j+n,j-1)} \times \left\{1 - \frac{L_0\{X(t_j) - f[X^*(t_j)] - X(t_{j-1}) + f[X^*(t_{j-1})]\}}{\sum_{i=j+1}^{N} l^a_{(i,j-1)}}\right\}, \tag{21}$$

where

$$X^*(t_j) = \frac{\sum_{i=j+1}^{N} l_{0i}}{L_0}. \tag{22}$$

Equation 21 is equivalent to equation 8 of Yu and Sotirchos (1987) and can be explained as follows: $L_0\{X(t_j) - f[X^*(t_j)]\}$ is the length of open and inaccessible pores at t_j, and $L_0[(X(t_{j-1}) - f(X^*(t_{j-1}))]$ is the length of open and inaccessible pores at t_{j-1}. Their difference is the length of open and inaccessible pores created at time t_j. The term in the denominator

$$\sum_{i=j+1}^{N} l^a_{(i,j-1)}$$

is the length of the active groups over which the inaccessible pores created at t_j are distributed. It follows that $1-\alpha$ is the fraction of accessible pores at t_{j-1} that remains accessible at t_j, where

$$\alpha = \frac{L_0\{X(t_j) - f[X^*(t_j)] - X(t_{j-1}) + f[X^*(t_{j-1})]\}}{\sum_{i=j+1}^{N} l^a_{(i,j-1)}}$$

gives the fraction of accessible pores that becomes inaccesible at t_j.

It should be noted that Eq. 21 is equivalent to

$$l^a_{(j+n,j)} = l_{(j+n)0}\left\{\frac{f(X^*(t_j))}{X^*(t_j)}\right\}, \tag{21a}$$

which one would use ignoring the trapping effect. The inclusion of the trapping effect does not influence the distribution of open and accessible pores. The difference is in the distribution and number of open nonaccessible pores, and the number of blocked pores. The lengths $\{l^n_{(j+1,j)}, \ldots, l^n_{(N,j)}\}$ of open inaccessible pores of radii $\{R_{0j+1}-(R_{0j}-r^*), \ldots, R_{0N}-(R_{0j}-r^*)\}$ that are formed at t_j are given by

$$l^n_{(i,j)} = l^a_{(i,j-1)} - l^a_{(i,j)}. \tag{23}$$

These pores are kept unchanged in the subsequent pore closures. If the trapping effect was ignored, then the deposit in the pores would be allowed to continue growing.

Equations 21, 22, and 23 provide all the information required for the computation of accessible and inaccessible lengths every time that a new group of pores becomes closed. At $t=0$ the various lengths are $l^n_{(i,0)}=0$ and $l^a_{(i,0)}=l_{0i}$. Ignoring pore overlapping, the accessible surface area at time t $(t_j \le t < t_{j+1})$ is calculated as follows:

$$A = 2\pi \sum_{i=j+1}^{N} l^a_{(i,j)}(R_{0i}-q). \tag{24}$$

For simplicity a Bethe-type lattice was chosen to represent the pore network. Treating the coordination number, z, of the Bethe lattice as an adjustable parameter affords sufficient flexibility to mimic the behavior of more realistic networks. Accessibility functions of various Bethe lattices are given in Figure 1. In order to model high percolation thresholds decorated Bethe lattices were used where a bond of the regular Bethe lattice is replaced by a bond graph consisting of two bonds in series. The calculations of the accessibility function of the lattices were performed based on the results of Fisher and Essam (1961).

Effective Diffusivity for Simple Lattices. For the evaluation of the effective diffusivity we follow the approach of Stinchcombe (1974). For simple (nondecorated) lattice and for

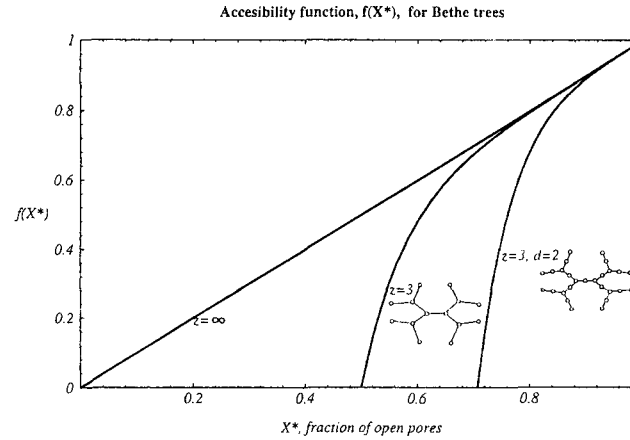

Figure 1. Accessibility functions for simple Bethe lattices with $z=\infty$ and $z=3$, and decorated Bethe lattice ($z=3$, $d=2$).

Knudsen diffusion the conductance of a single bond is related to its size by the relationship

$$u(r) = \pi K\left(\frac{T}{M}\right)^{1/2} l^{-1} r^3 = r^3 Q, \tag{25}$$

where M is the molecular weight; K, the constant in the Knudsen diffusion coefficient; and l the length of the pore. The average conductivity, σ, of a Bethe tree is given by

$$\sigma = -zx. \tag{26}$$

Stinchcombe (1974) provided an integral equation for the exact evaluation of x as well as a simplified procedure for determining x to order $(z-1)^{-4}$. In this work x is determined from the following integral equation (Stinchcombe, 1974; Yortsos and Sharma, 1986), which is the leading-order effective medium approximation:

$$0 = \int_0^\infty dug(u)\frac{u - \dfrac{z-1}{z(z-2)}\sigma}{u + \dfrac{(z-1)}{z}\sigma} = \int_0^\infty dug(u)\left[\frac{u(z-1)}{u-(z-1)x} - 1\right]\frac{1}{(z-2)}. \tag{27}$$

This expression provides a good approximation except in the immediate neighborhood of the percolation limit. It also gives zero conductance at the percolation limit.

The analysis by Stinchcombe (1974) is valid for the (random) process without trapping. Since the process with trapping and the process without trapping have identical distributions of open-accessible pores, they have the same conductance. Thus, the results of Stinchcombe (1974) that are applicable to the process without trapping also provide the conductance for the process with trapping. Application of these results for the present case involve a discrete distribution $g(u)$ given by the equation (Yortsos and Sharma, 1986):

$$g(u)=[1-X^*(t_j)]\delta(u)+X^*(t_j)G(u), \qquad (28)$$

where $G(u)$ is the conductance distribution function of the open (accessible and inaccessible) pores for the process with no trapping:

$$G(u)du=\frac{1}{X^*(t_j)}\left[\left\{\sum_{i=j+1}^{N}\frac{l^a_{(i,j)}}{L_0}\delta\left[u-Q(R_{0i}-q-r^*)^3\right]\right\}+\sum_{i=j+1}^{N}\frac{(l_{0i}-l^a_{(i,j)})}{L_0}\delta\left[u-Q(R_{0i}-R_{0j})^3\right]\right]du. \qquad (29)$$

Using Eqs. 28 and 29, Eq. 27 becomes an algebraic equation in x:

$$X^*(t_j)-1+\sum_{i=j+1}^{N}\frac{l^a_{(i,j)}}{L_0}\left[\frac{Q(R_{0i}-q-r^*)^3(z-1)}{Q(R_{0i}-q-r^*)^3-(z-1)x}-1\right]+\sum_{i=j+1}^{N}\frac{(l_{0i}-l^a_{(i,j)})}{L_0}\left[\frac{Q(R_{0i}-R_{0j})^3(z-1)}{Q(R_{0i}-R_{0j})^3-(z-1)x}-1\right]=0 \qquad (30)$$

for $R_{0j}-r^*<q<R_{0j+1}-r^*$. A first estimate for x can be obtained (Reyes and Jensen, 1985) from

$$x=(X^*(t_j)-p_c)\left\{\int_0^{\infty}\frac{G(u)}{u}du\right\}^{-1}.$$

The effective diffusivity normalized by its value at the beginning of the process is given by

$$\frac{D_{\text{eff}}(t_j)}{D^0_{\text{eff}}}=\frac{x(t_j)}{x(0)}. \qquad (31)$$

Decorated lattices

Calculation of Accessible Surface Area. For the decorated Bethe lattice where each of the bonds of the lattice is replaced by a compound bond consisting of two segments in series the calculations for the accessible surface area are performed as in the case for the simple lattice, but using in the calculations (Eq. 21) the accessibility function of the decorated lattice (see Figure 1). This way all the accessible segments are accounted for their contribution to the surface area.

Calculation of Effective Diffusivity. For the calculation of diffusivity we consider the open and accessible bonds of the original nondecorated lattice. From the distribution of segments we derive the initial distribution of bond conductances. From the N types of segments with radii $R_{01}<R_{02}<\cdots<R_{0n}$ and lengths $l_{01}, l_{02}, \ldots, l_{0N}$ one has $[N(N+1)]/2$ types of bonds with lengths:

$$l_{1,1,0}=\frac{l^2_{01}}{L^2_0}L_0 \quad l_{1,2,0}=\frac{2l_{01}l_{02}}{L^2_0}L_0\cdots l_{1,N,0}=\frac{2l_{01}l_{0N}}{L^2_0}L_0$$
$$l_{2,2,0}=\frac{l^2_{02}}{L^2_0}L_0\cdots l_{2,N,0}=\frac{2l_{02}l_{0N}}{L^2_0}L_0$$
$$\vdots$$
$$l_{N,N,0}=\frac{l^2_{0N}}{L^2_0}L_0.$$

These segments have the corresponding conductances:

$$u_{1,1,0}=\frac{QR^3_{01}}{2} \qquad u_{1,2,0}=\frac{QR^3_{01}R^3_{02}}{R^3_{01}+R^3_{02}}\cdots u_{1,N,0}=\frac{QR^3_{01}R^3_{0N}}{R^3_{01}+R^3_{0N}}$$
$$u_{2,2,0}=\frac{QR^3_{02}}{2}\cdots u_{2,N,0}=\frac{QR^3_{02}R^3_{0N}}{R^3_{02}+R^3_{0N}}$$
$$\vdots$$
$$u_{N,N,0}=\frac{QR^3_{0N}}{2}.$$

At time t with $t_j<t<t_{j+1}$ all segments with initial radii $R_{0i}\le R_{0j}$ are either closed or open but inaccessible, consequently all bonds that contain such segments are closed or inaccessible with regard to their contribution in the effective diffusivity.

At time t, $t_j<t<t_{j+1}$, one has accessible bonds with lengths:

$$l^a_{j+1,j+1,j} \quad l^a_{j+1,j+2,j}\cdots l^a_{j+1,N,j}$$
$$l^a_{j+2,j+2,j}\cdots l^a_{j+2,N,j}$$
$$\vdots$$
$$l^a_{N,N,j}$$

with conductance

$$u^a_{i,k,j}=\frac{Q(R_{0i}-q-r^*)^3(R_{0k}-q-r^*)^3}{(R_{0i}-q-r^*)^3+(R_{0k}-q-r^*)^3},$$

corresponding to the bonds with length $l^a_{i,k,j}$.

At the same time one also has j groups of open inaccessible bonds:

$$l^n_{i+1,i+1,i} \quad l^n_{i+1,i+1,i}\cdots l^n_{i+1,N,i}$$
$$l^n_{i+2,i+2,i}\cdots l^n_{i+2,N,i}$$
$$\vdots$$
$$l^n_{N,N,i}$$

with $i=1, 2, \ldots, j$. The conductance corresponding to the bonds with length $l^n_{i,k,j}$ is

$$u^n_{i,k,j}=\frac{Q(R_{0i}-R_{0j})^3(R_{0k}-R_{0j})^3}{(R_{0i}-R_{0j})^3+(R_{0k}+R_{0j})^3}.$$

By the same reasoning as used to obtain Eq. 20, the fraction of open bonds (accessible and inaccessible) is

$$X(t_j) = 1 - \frac{\sum_{i=1}^{j} \sum_{k=i}^{N} l^a_{i,k,i-1}}{L_0}. \tag{32}$$

The fraction of open bonds for the process without trapping is

$$X^*(t_j) = 1 - \frac{\sum_{i=1}^{N} \sum_{k=i}^{N} l_{i,k,0}}{L_0} = \frac{\left(\sum_{i=1}^{N} l_{0i}\right)^2}{L_0^2}. \tag{33}$$

The open and accessible bonds at t_j have lengths

$$l^a_{j+n,k,j} = l^a_{j+n,k,j-1} \times \left\{1 - \frac{L_0\{X(t_j) - f(X^*(t_j) - X(t_{j-1}) + f[X^*(t_{j-1})]\}}{\sum_{i=j+1}^{N} \sum_{k=i}^{N} l^a_{i,k,j-1}}\right\} \tag{34}$$

with $k = j+n, \ldots, N$ and $j+n = 1, \ldots, N$, where f is the accessible function of the simple lattice. This equation is analogous to Eq. 21 and is justified similarly. Finally, the nonaccessible bond lengths are given by

$$l^n_{j+n,k,j} = l^a_{j+n,k,j-1} - l^a_{j+n,k,j}. \tag{35}$$

Equations 32–35 provide the information needed in order to calculate accessible and inaccessible lengths of bonds every time that a new group of segments becomes closed.

Equations 26, 27, 28, and 31 are used, then, to calculate the effective diffusivity by an equation analogous to Eq. 29:

$$G(u)du = \frac{1}{X^*(t_j)} \left\{ \left[\sum_{i=j+1}^{N} \sum_{k=i}^{N} \frac{l^a_{i,k,j}}{L_0} \delta(u - u^a_{i,k,j}) + \sum_{i=j+1}^{N} \sum_{k=i}^{N} \frac{l_{i,k,0} - l^a_{i,k,j}}{L_0} \delta(u - u^n_{n,k,i}) \right] \right\} du. \tag{36}$$

Similarly to the simple lattice the conductance distribution function is calculated for the process without trapping using the length distributions defined by Eq. 34 and the appropriate pore radii.

Numerical Results and Discussion

Simulations were performed for SiO_2 deposition in the opposing reactants geometry (ORG) at 400–800°C. The rate constants as estimated in Kim and Gavalas (1994) are:

$$k_1 = (1.76 \times 10^{15}) e^{-29{,}700/RT} \quad \text{and}$$

$$k_2 = (1.09 \times 10^{11}) e^{-19{,}800/RT}$$

The surface concentration of silanol groups (−OH) on Vycor glass after heating at 600°C was estimated as 1.5 OH/nm^2 (Kim and Gavalas, 1994). Other reports, however, give values as high as 5 OH/nm^2. The initial −OH concentration also depends on the time of dehydroxylation in the initial heat treatment of the substrate. In the simulations we used values between 1.5 and 3 −OH/nm^2. The Nusselt number was estimated around 4 as previously (Tsapatsis and Gavalas, 1992). The parameter S^* was varied between 5 and 10 sites/nm^2. Due to the lack of sufficient experimental data, refinement of this parameter was not attempted. Permeation data suggest that the deposited material is highly defective immediately after deposition; therefore, values for the deposit density were varied between 1.5 and 1.8 g/cm^3, considerably lower than typical SiO_2 densities of 2.1 g/cm^3.

The time evolution equations (Eqs. 10, 11, and 14) were integrated using the fourth-order Runge-Kutta routine. Each evaluation of the righthand side of these equations required solution of the linear boundary value problem, Eqs. 12–13, 16–19. This solution was carried out by spatial discretization (finite differences) and solution of the resulting linear system by Gaussian elimination.

Diffusivities and accessible surface area are needed for each deposition time and are calculated by the following procedure. It is first noticed that the pore evolution problem can be solved in terms of the local deposit thickness, q, independently of Eqs. 10–19. A table is thus created giving local diffusivities and accessible surface areas as functions of the deposit thickness for various lattices by using Eqs. 20–26 and 30–31 for the simple lattices, and Eqs. 32–35 and 26–28, 31, 36 for the decorated lattices. In these calculations the pore-size distribution of Vycor, provided by the manufacturer (Corning Inc.), was discretized in increments of 1 Å. For D^0_{eff} the experimentally determined value is used. The tabulated values of diffusivities and accessible surface area are retrieved during the simulation once the local value of q is specified. Each run was terminated when interruption of connectivity took place at some point in the substrate. Since $SiCl_4$ and H_2O have different sizes, the simulations were terminated when the connectivity is interrupted for the larger molecule, $SiCl_4$. At that time H_2O is still able to diffuse in the network toward the chloride side. That will lead to an increase of the deposit thickness. In the model we do not account for this characteristic of the opposing reactants geometry.

Simulations were performed for *regular* Bethe lattices with coordination number 3 ($z = 3$) and *decorated* Bethe lattices with coordination number 3 where a compound bond consists of two bonds in series ($z = 3$, $d = 2$). Use of decorated lattices allows the flexibility to include cross-section variations within a single pore segment (bond).

Figure 2 shows the calculated accessible length, volume, and surface-area fractions, as well as the normalized diffusivity vs. the fraction of open pores for a Bethe tree with $z = 3$ (Figure 2a) and a Bethe tree with $z = 3$, $d = 2$ (Figure 2b). Figure 2a1 shows results including the trapping effect, while Figure 2a2 shows the corresponding results for the process without trapping. As can be seen at the percolation threshold the fraction of residual open pores is higher for the process with trapping. For Vycor glass the difference in the calculated residual volumes is small: for the simple lattice ($z = 3$)

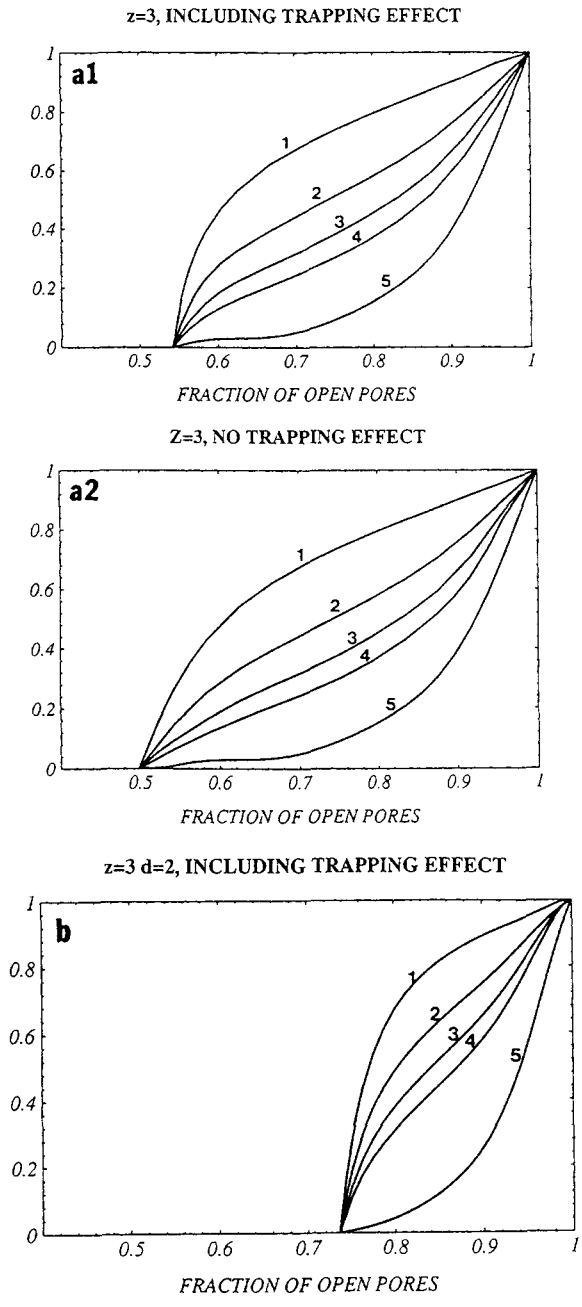

Figure 2. Accessible length fraction (1); accessible surface-area fraction (2); accessible volume fraction (3); normalized diffusivity from parallel-pore formulation (4); normalized diffusivity from effective medium formulation (5) vs. fraction of open pores.

(a1) Simple Bethe lattice with $z = 3$, calculations including trapping effect; (a2) simple Bethe lattice with $z = 3$, calculations with no trapping effect; (b) decorated Bethe lattice with $z = 3$ and $d = 2$, calculations including trapping effect.

the residual volume is 0.05 cm^3/g including trapping and 0.042 cm^3/g without trapping. In the case of the decorated lattice ($z = 3$, $d = 2$) the corresponding values are 0.094 and 0.082. The diffusivity, accessible surface area, and accessible volume are identical for both computational schemes. In Figure 2 the diffusivity values calculated using a simple parallel model are also included for comparison. This calculation was performed using the accessible bonds only and ignoring changes in tortuosity:

$$\frac{D_{\text{eff}}(t_j)}{D^0_{\text{eff}}} = \frac{\sum_{i=j+1}^{N} l^a_{(i,j)}(R_{0i} - q - r^*)^3}{\sum_{i=j+1}^{N} l_{0i}(R_{0i})^3}.$$

The parallel-pore approach overestimates the diffusivity, since it does not account for the increase of tortuosity with pore blockage. However, simulations of deposition (not shown here) performed using the latter simpler approach for calculating diffusivity do not show substantial differences from simulations performed using the more detailed approach presented here. This lack of sensitivity is probably due to the narrow pore-size distribution of Vycor glass and to the fact that connectivity effects are not important at the early stages of deposition, as elaborated further in the discussion of Figure 3.

Figure 3 shows the calculated deposit densities at the end of deposition (reaction at 800°C using 30% chloride and 10%

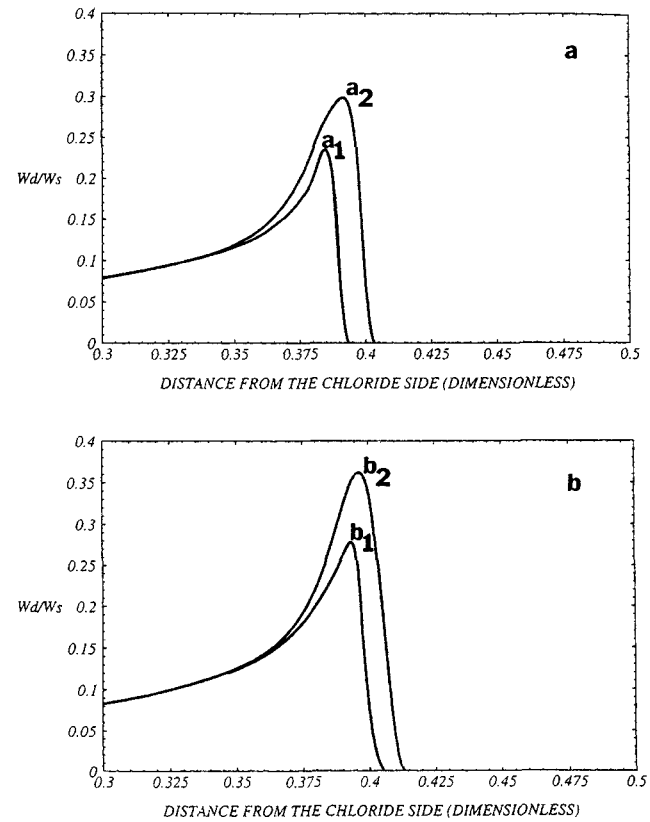

Figure 3. Deposit profiles at the end of deposition for ORG reaction conditions: 800°C, 10% H_2O, and 30% $SiCl_4$.

(a) Curve a_1 ($z = 3$, $d = 2$), $v = 40$ cm^3/mol; curve a_2: ($z = 3$), $v = 40$ cm^3/mol; (b) curve b_1: ($z = 3$, $d = 2$), $v = 33$ cm^3/mol; curve b_2: ($z = 3$), $v = 33$ cm^3/mol. Times for pore plugging: curve a_1—34 min; curve a_2—38 min; curve b_1: 38.5 min; curve b_2—43.5 min.

water). Two different deposit densities were used in the simulations, 1.5 and 1.8 g/cm^3, corresponding to deposit molar volumes of $\upsilon = 40$ and 33 cm^3/mol, respectively. The influence of pore-structure connectivity is demonstrated by including results for a simple Bethe lattice $z = 3$ and a decorated Bethe lattice ($z = 3$, $d = 2$) for each deposit density. As expected the lower density deposit leads to faster pore constriction and pore plugging. Faster pore plugging also takes place when one accounts for pore constrictions using a decorated lattice. The term pore plugging is used here to indicate reaching the percolation limit at which the effective diffusivity of $SiCl_4$ is zero.

Figure 3a shows the calculated deposit densities normalized by the substrate density (Wd/Ws: deposit over substrate weight ratio) for $z = 3$ and ($z = 3$, $d = 2$) using $\upsilon = 40$ cm^3/mol. The normalized density is smaller for the decorated Bethe lattice due to pore plugging at a larger void fraction. Moreover, the deposit profile around the region of maximum deposition is sharper. Pore connectivity effects manifest themselves during the final stages of deposition and thus no differences in the profiles are observed in the tail of the profile, which is far from the percolation threshold. For the same reason the differences in time for pore plugging are small. Using the lower molar volume, $\upsilon = 33$ cm^3/mol yields a qualitatively similar profile but with a higher peak. Clearly, a lower molar volume requires an increased amount of deposit in order to fill the same pore volume (Figure 3b). The maximum deposit density was estimated previously from TGA and EPMA measurements (Tsapatsis and Gavalas, 1994). The experimental density can be matched by many combinations of lattices and molar volumes, and in order to meaningfully compare experimentally determined profiles with simulation, these two parameters should be independently estimated. Unfortunately, there was not sufficient information available to obtain these independent estimates. It is interesting to note, however, that the simulation results show a different effect of the deposit molar volume from that of the lattice, on the deposit profile. The molar volume influences the maximum deposit density, but has a minimal effect on the width of the deposit peak, as is evident if one compares the width of the deposit at a deposit density of 90% of the maximum value. On the other hand, a similar comparison for the effect of network connectivity shows a much more pronounced effect: the width at a deposit density of 90%, the maximum value for the decorated lattices, is almost half of that of the simple lattice. These results suggest that the deposit profile in a substrate with a high percolation threshold will be sharper in the neighborhood of maximum deposition. The effects of network connectivity (coordination number) shown in Figure 3 are modest because of the relatively narrow pore size distribution of Vycor glass. These effects are expected to be more pronounced for wider pore-size distributions.

Figure 4 shows the influence of the parameter S^* on the deposit profiles. Two values were used corresponding to a maximum of 5 and 10 accessible surface sites per nm^2. As S^* increases, pore plugging takes place faster and the deposit profile moves toward the chloride side.

Figure 5 shows the influence of the initial concentration of OH species on the final deposit profile. A lower initial OH concentration leads to faster pore plugging. This surprising result demonstrates the complicated interplay of transport

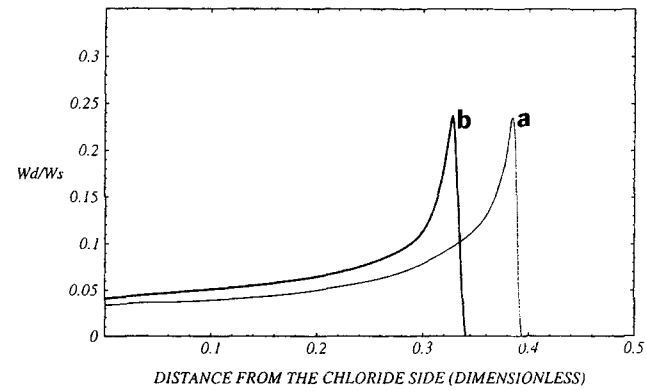

Figure 4. Influence of kinetic parameter S^* on the deposit profiles.

Curve a: $S^* = 5$/nm^2 (time for pore plugging = 34 min); curve b: $S^* = 10$/nm^2 (time for pore plugging = 32 min). The molar volume is $\upsilon = 40$ cm^3/mol and the lattice has $z = 3$, $d = 2$. Other parameters as in Figure 3.

and transient kinetics during deposition. An explanation is possible by considering the reaction of $SiCl_4$ with the initial OH species in the absence of water. That reaction leads to the formation of the first deposit layer that is responsible for the tail of the deposit profile. As the initial number of OH species is decreased, this depletion effect is less pronounced and the chloride penetrates more deeply into the substrate, decreasing the overall deposition time and producing a sharper deposit peak. A pseudo-steady-state approximation for the surface species cannot predict such behavior. Equations A17–A21 (see the Appendix), although incorporating the effect of surface coverage, do not utilize any information regarding the initial concentration of surface species.

To demonstrate the importance of transient kinetics further, a more extreme case was examined in the following simulation. Before the ORG deposition the substrate surface was pretreated with $SiCl_4$ in the absence of water so that all OH groups were replaced with Cl groups according to reaction 2. The simulation of deposition was then started. The resulting profile shown in Figure 6 is very different from the profile

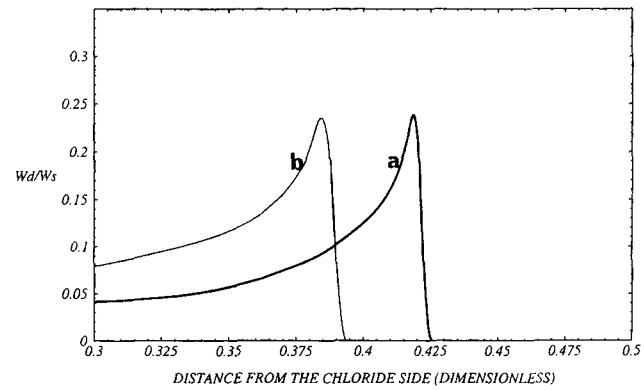

Figure 5. Influence of initial OH concentration on the deposit profiles.

a: 1.5 OH/nm^2 (time for pore plugging = 28 min); b: 3 OH/nm^2 (time for pore plugging = 34 min). $S^* = 5$/nm^2. Other parameters as in Figure 4.

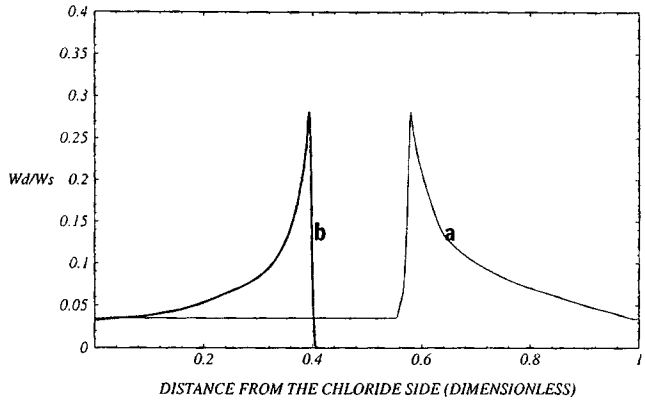

Figure 6. a. Deposit profile at the end of deposition after dehydroxylation (time for pore plugging = 65 min); b: corresponding profile at the end of deposition without prior dehydroxylation (time for pore plugging = 38.5 min) ($S^* = 5/nm^2$, $v = 33$ cm^3/mol; other parameters as in Figure 4).

calculated for deposition without prior chlorination. Qualitatively similar behavior has been observed experimentally and reported before (Tsapatsis and Gavalas, 1992). The sensitivity of the deposit profile on the initial state of the substrate surface is a characteristic of the ORG deposition and is not expected when both reactants are introduced from the same side of the substrate.

Finally, the influence of reaction temperature is shown in Figure 7. Lower temperatures decrease the reaction rate and result in thicker reaction zones. At 400°C the deposit is spread over the whole thickness of the substrate. Temperatures higher than 600°C are needed for the formation of a thin deposit layer, in agreement with experimental observations (Tsapatsis et al., 1991).

The simulation results are in qualitative agreement with the experimental observations reported by Tsapatsis and Gavalas (1992, 1994). Quantitative comparison of model predictions with experimental results is not attempted here in view of the uncertainties involved in the estimation of model

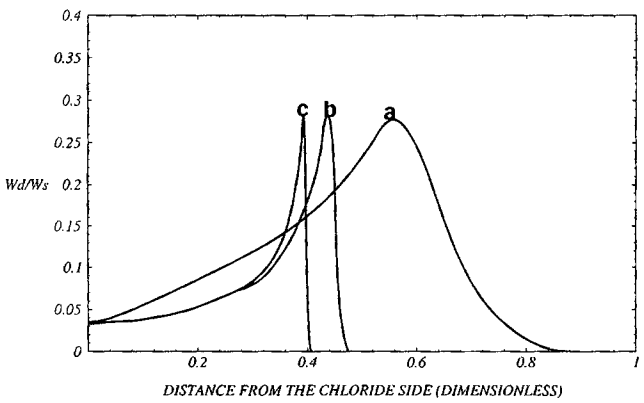

Figure 7. Influence of deposition temperature on deposit profiles.

a. 400°C; b. 600°C; c. 800°C. 3 OH/nm^2. Other parameters as in Figure 6.

parameters and the lack of systematic variation of experimental parameters. An additional implication that emerges from the simulation and the importance of the transient kinetics that renders most of our previous experimental data not appropriate for quantitative comparison with the model simulations is the following: the initially employed experimental procedure involved interruption of deposition for permeance measurements followed by other deposition cycles. It is evident that this procedure, depending on the deposition conditions used, can lead to different deposit profiles compared with a once-through deposition scheme. Nevertheless, the model can be used to gain insight on the deposition process. For instance, Figure 3 indicates a considerable effect of substrate connectivity on deposit thickness with potential implications in the selection of appropriate substrates to minimize deposit thickness. Figures 5 and 6 show that the deposition conditions leading to an increased time for pore plugging do not necessarily produce a thicker deposit at the region of maximum deposition. This lack of correlation between time for pore plugging and deposit thickness is due to the fact that most of the reaction time involves deposit buildup away from the region of maximum deposition.

Conclusions

A model has been developed for the deposition of silica in porous Vycor using $SiCl_4$ hydrolysis in an opposing reactants geometry. The reaction mechanism was based on previous studies involving reaction of the gaseous chloride with silanol sites on the surface and reaction of water vapor with chloride sites on the surface. The transient kinetics associated with these reactions were introduced into a continuum model describing diffusion and pore closure making use of percolation theory concepts. It was found that for typical deposition conditions network connectivity has a modest effect on the time for pore plugging and a more pronounced effect on the deposit thickness at the region of maximum deposition, but does not affect the location of the deposit. It was also shown that transient kinetics are essential for the description of deposit growth in the mesoporous Vycor substrate.

Acknowledgments

The authors appreciate funding of this project by the Department of Energy under the University Coal Research Program, Grant DE-FG22-92PC92525. One of the authors (M. T.) acknowledges partial support through a David and Lucile Packard Foundation Fellowship in Science and Engineering. Professor Sotirchos provided helpful suggestions.

Notation

C_i^0 = chloride or water concentration at the bubbler, mol/cm^3
d = diameter of Vycor tube, cm
d' = equivalent hydraulic diameter of outside flow, cm
D_i = Knudsen diffusivity of species i, cm^2/min
$D_{i,\text{bulk}}$ = binary diffusivity of species i, cm^2/min
D_i = dimensionless diffusivity
L = thickness of substrate Vycor tube, cm
L_0 = total initial length of pores, cm/cm^3
l_{0i} = initial length of pores with initial radius R_{0i}, cm/cm^3
$l_i = \dfrac{\text{Nu } Di, bulk}{d}$ mass-transfer coefficient, cm/min
$l_i' = \dfrac{\text{Nu}' Di, bulk}{d'}$ mass-transfer coefficient, cm/min

M_i = molecular weight of species i
Nu = Nusselt number
q° = initial thickness of deposit layer perpendicular to pore wall, cm
R = gas constant
$S_{OH,ss}$ = steady-state –OH concentration, mol/cm^2 or sites/nm^2
$S_{Cl,ss}$ = steady-state –OH concentration, mol/cm^2 or sites/nm^2
s = dimensionless accessible surface area
s_{OH} = dimensionless –OH concentration
s_{Cl} = dimensionless –Cl concentration
T = temperature, K
u_i = dimensionless gas concentration
x = distance measured from inside wall of substrate tube, cm
z = dimensionless distance measured from inside wall of substrate tube (Chloride side)
ϵ_0 = initial void fraction of substrate
ϵ = void fraction of substrate
θ = dimensionless deposit thickness
τ^* = dimensionless time
Φ_1 = Thiele modulus
ψ = ratio of gaseous to surface species concentration

Literature Cited

Arbabi, S., and M. Sahimi, "Computer Simulations of Catalyst Deactivation—1. Model Formulation and Validation," *Chem. Eng. Sci.*, **46**, 1739 (1991).

Carolan, M., and J. N. Michaels, "Chemical Vapor Deposition of Yttria Stabilized Zirconia on Porous Substrates," *Solid State Ionics*, **25**, 207 (1987).

Efthimiadis, E. A., and S. V. Sotirchos, "Reactivity Evolution during Sulfidation of Porous Zinc Oxide," *Chem. Eng. Sci.*, **48**, 829 (1993).

Fisher, M. E., and J. W. Essam, "Some Cluster Size and Percolation Problems," *J. Math. Phys.*, **2**(4), 609 (1961).

Kim, S. J., and G. R. Gavalas, "Thermogravimetric Study of the Reactions of Chlorosilanes with the Surface of Vycor Glass," *J. Colloid Interface Sci.*, **161**, 6 (1993).

Lin, Y. S., and A. J. Burggraaf, "Modeling and Analysis of CVD Processes in Porous Media for Ceramic Composite Fabrication," *Chem. Eng. Sci.*, **46**, 3067 (1992).

Mace, O., and J. Wei, "Diffusion in Random Particle Models for Hydrodemetalation Catalysts," *Ind. Eng. Chem. Res.*, **30**, 909 (1991).

Mohanty, K. K., J. M. Ottino, and H. T. Davis, "Reaction and Transport in Disordered Media: Introduction of Percolation Concepts," *Chem. Eng. Sci.*, **37**, 905 (1982).

Reyes, S., and K. F. Jensen, "Percolation Concepts in Modeling of Gas-Solid Reactions—III. Application to Sulfation of Calcined Limestone," *Chem. Eng. Sci.*, **42**, 565 (1987).

Sahimi, M., "Fractal Dimension in a Percolation Model of Fluid Displacement," *Phys. Rev. Lett.*, **55**, 1698 (1985).

Sahimi, M., G. R. Gavalas, and T. T. Tsotsis, "Statistical and Continuum Models of Fluid-Solid Reactions in Porous Media," *Chem. Eng. Sci.*, **45**, 1443 (1990).

Sahimi, M., and T. T. Tsotsis, "A Percolation Model of Catalyst Deactivation by Site Coverage and Pore Blockage," *J. Catal.*, **96**, 552 (1985).

Sotirchos, S. V., and S. Zarkanitis, "A Distributed Pore Size and Length Model for Porous Media Reacting with Diminishing Porosity," *Chem. Eng. Sci.*, **48**(8), 1487 (1993).

Stinchcombe, R. B., "Conductivity and Spin-wave Stiffness in Disordered Systems—An Exactly Soluble Model," *J. Phys. C: Solid State Phys.*, **7**, 179 (1974).

Tsapatsis, M., and G. R. Gavalas, "A Kinetic Model for Membrane Formation by CVD of SiO_2 and Al_2O_3," *AIChE J.*, **38**, 847 (1992).

Tsapatsis, M., and G. R. Gavalas, "Structure and Aging Characteristics of H_2-Permselective SiO_2-Vycor Membranes," *J. Memb. Sci.*, **87**, 281 (1994).

Tsapatsis, M., S. Kim, S. W. Nam, and G. R. Gavalas, "Synthesis of Hydrogen Permselective SiO_2, TiO_2, Al_2O_3 and B_2O_3 Membranes from the Chloride Precursors," *Ind. Eng. Chem. Res.*, **30**, 2152 (1991).

Yortsos, Y. C., and M. Sharma, "Application of Percolation Theory to Noncatalytic Gas-Solid Reactions," *AIChE J.*, **32**(1), 46 (1986).

Yu, H.-C., and S. V. Sotirchos, "A Generalized Pore Model for Gas-Solid Reactions Exhibiting Pore Closure," *AIChE J.*, **33**(3), 382 (1987).

Xomeritakis, G., and Y. S. Lin, "Chemical Vapor Deposition of Solid Oxides in Porous-Media for Ceramic Membrane Preparation or Modification-Comparison of Experimental Results with Semianalytical Solutions," *Ind. Eng. Chem. Res.*, **33**, 2607 (1994a).

Xomeritakis, G., and Y. S. Lin, "Chemical Vapor Deposition of Solid Oxides in Porous-Media for Ceramic Membrane Preparation or Modification-Explicit Solutions for Deposition Characteristics," *Chem. Eng. Sci.*, **49**, 3909 (1994b).

Zarkanitis, S. E., E. A. Efthimiadis, and S. V. Sotirchos, "Experimental Evaluation of Distributed Pore Size Models for Gas-Solid Reactions with Solid Product," *Chem. Eng. Sci.*, **45**, 2761 (1990).

Appendix

The reaction diffusion problem is formulated as follows:

$$\frac{\partial C_1}{\partial t} - \frac{\partial}{\partial x}\left[D_1(\epsilon)\frac{\partial C_1}{\partial x}\right] = -k_1 C_1 A S_{OH} \tag{A1}$$

$$\frac{\partial C_2}{\partial t} - \frac{\partial}{\partial x}\left[D_2(\epsilon)\frac{\partial C_2}{\partial x}\right] = -k_2 C_2 A S_{Cl} \tag{A2}$$

$$\frac{\partial_{OH}}{\partial t} = -k_1 C_1 S_{OH} + k_2 C_2 S_{Cl} - \frac{2}{S^*} k_1 C_1 S_{OH^2} \tag{A3}$$

$$\frac{\partial S_{Cl}}{\partial t} = 3k_1 C_1 S_{OH} - k_2 C_2 S_{Cl} - \frac{2}{S^*} S_{Cl} k_1 C_1 S_{OH} \tag{A4}$$

$$\frac{\partial q}{\partial t} = \upsilon k_1 C_1 S_{OH}. \tag{A5}$$

The preceding equations are made dimensionless using the variables in the Notation section to assess the magnitude of certain terms. The dimensionless equations are:

$$\frac{\partial u_1}{\partial \tau^*} - \frac{\partial}{\partial z}\left(D_1(\epsilon)\frac{\partial u_1}{\partial z}\right) = -\Phi_1^2 u_1 ss_{OH} \tag{A6}$$

$$(D_{10}/D_{20})\frac{\partial u_2}{\partial \tau^*} - \frac{\partial}{\partial z}\left(D_2(\epsilon)\frac{\partial u_2}{\partial z}\right) = -(k_2/k_1)(D_{10}/D_{20})\Phi_1^2 u_2 ss_{Cl} \tag{A7}$$

$$\frac{\partial s_{OH}}{\partial \tau^*} = -\psi\Phi_1^2 u_1 s_{OH} + (k_2/k_1)\psi\Phi_1^2 u_2 s_{Cl} - \frac{2S_{OH}^0}{S^*}\psi\Phi_1^2 u_1 s_{OH}^2 \tag{A8}$$

$$\frac{\partial s_{Cl}}{\partial \tau^*} = 3\psi\Phi_1^2 u_1 s_{OH} - (k_2/k_1)\psi\Phi_1^2 u_2 s_{Cl} - \frac{2S_{OH}^0}{S^*}\psi\Phi_1^2 u_1 s_{Cl} s_{OH} \tag{A9}$$

$$\frac{\partial \theta}{\partial \tau^*} = \frac{\upsilon S_{OH}^0}{a}\psi\Phi_1^2 u_1 s_{OH}. \tag{A10}$$

The parameter ψ defined by

$$\psi = \frac{C_1^0}{A^0 S_{OH}^0} \tag{A11}$$

is the ratio of gaseous and surface species concentrations, and is much smaller than unity for typical deposition conditions. This means that S_{Cl}, S_{OH}, and θ change on a time scale significantly longer than the time scale for gaseous concentration changes, suggesting that the quasi-steady-state approximation can be applied to the gaseous concentrations. Thus the equations in dimensional form are simplified to

$$\frac{\partial}{\partial x}\left[D_1(\epsilon)\frac{\partial C_1}{\partial x}\right] = k_1 C_1 A S_{OH} \tag{A12}$$

$$\frac{\partial}{\partial x}\left[D_2(\epsilon)\frac{\partial C_2}{\partial x}\right] = k_2 C_2 A S_{Cl} \tag{A13}$$

$$\frac{\partial S_{OH}}{\partial t} = -k_1 C_1 S_{OH} + k_2 C_2 S_{Cl} - \frac{2}{S^*} k_1 C_1 S_{OH}^2 \tag{A14}$$

$$\frac{\partial S_{Cl}}{\partial t} = 3k_1 C_1 S_{OH} - k_2 C_2 S_{Cl} - \frac{2}{S^*} S_{Cl} k_1 C_1 S_{OH} \tag{A15}$$

$$\frac{\partial q}{\partial t} = \upsilon k_1 C_1 S_{OH}. \tag{A16}$$

For typical conditions of deposition, the term $\upsilon S_{OH}^0/a$ in Eq. A10 is of order 0.1 to 1, suggesting that the pseudo-steady-state approximation for the surface species cannot be used. This is the case here because the typical pore radius, a, of porous Vycor is about 2 nm. For deposition on a macroporous substrate, this term will be much smaller than unity, justifying the elimination of Eqs. A8 and A9. In that case, the equations would be

$$\frac{\partial}{\partial x}\left[D_1(\epsilon)\frac{\partial C_1}{\partial x}\right] = k_1 C_1 A S_{OH,SS} \tag{A17}$$

$$\frac{\partial}{\partial x}\left[D_2(\epsilon)\frac{\partial C_2}{\partial x}\right] = k_2 C_2 A S_{Cl,SS} \tag{A18}$$

$$\frac{\partial q}{\partial t} = \upsilon k_1 C_1 S_{OH,SS}, \tag{A19}$$

where the steady-state concentrations of surface species would be given by

$$S_{OH,SS} = \frac{-1-b+(b^2+1+10b)^{1/2}}{4c} \tag{A20}$$

$$S_{Cl,SS} = S^* - S_{OH,SS} \tag{A21}$$

with

$$b = \frac{k_2 C_2}{k_1 C_1} \quad \text{and} \quad c = \frac{1}{S^*}.$$

Manuscript received Dec. 15, 1995, and revision received Jan. 17, 1997.